Transient Kinetics and Intermediates Formed during the Electron Transfer Reaction Catalyzed by *Candida albicans* Estrogen Binding Protein[†]

James Buckman and Susan M. Miller*

Department of Pharmaceutical Chemistry, University of California School of Pharmacy, San Francisco, California 94143-0446

Received March 21, 2000; Revised Manuscript Received June 16, 2000

ABSTRACT: The transient kinetics of the reaction of the estrogen binding protein (EBP1) from *Candida albicans* in which hydride is transferred from NADPH to *trans*-2-hexenal (HXL) in two half-reactions were analyzed using UV−visible spectrophotometric and fluorometric stopped-flow techniques. The simplest model of the first half-reaction involves four steps including very rapid, tight binding ($K_d \leq 50$ nM) characterized by loss of NADPH fluorescence, subsequent rapid formation of a charge-transfer complex between NADPH and oxidized enzyme-bound flavin mononucleotide (FMN) cofactor, followed by rate-limiting reduction of the FMN, and finally dissociation of the oxidized pyridine nucleotide. The UV−visible absorbance behavior of this half-reaction is described by two apparent phases, with $k^f_{obs} = 355 \pm 6$ and $k^s_{obs} = 3.30 \pm 0.03$ s^{-1}, for the fast and slow phases, respectively. The reaction has also been evaluated in terms of the full, multi-equilibrium reaction scheme, and microscopic rate constants that lead to the observed behavior have been determined through convergent experimental techniques and computer simulation. Significant intrinsic kinetic isotope effects were noted on both the bond cleavage step and the preceding formation of the charge-transfer complex. The enzyme is reoxidized by transfer of hydride from the FMN to HXL in the second half-reaction that appears to consist of substrate binding to form a Michaelis-type complex and the subsequent chemical step. Characterization of the reaction in this simple manner allows determination of an apparent $K_d = 100 \pm 9$ μM for the reduced enzyme·HXL complex.

The estrogen binding protein (EBP1)[1] of *Candida albicans* was isolated because of its high, specific affinity for 17β-estradiol (*1*). To date, it represents the only estrogen binding activity identified in this organism, and, therefore, may represent a connection between the reported effects of estrogenic steroids on *C. albicans* (*2, 3*) and pathogenicity in humans. In addition to its high affinity for estrogens, we have demonstrated previously that EBP1 is an oxidoreductase that contains a redox-active flavin mononucleotide (FMN) cofactor (*4, 5*). Though the physiological substrates of EBP1 have not yet been identified, this enzyme has been demonstrated to catalyze the transfer of hydride from NADPH to a variety of α,β-unsaturated ketones and aldehydes. While estrogens do not serve as substrates for this protein, tight binding of these compounds in the active site has been shown to result in the inhibition of catalytic activity (*4*). In fact, this may be an important point of interaction between the physiology of the fungal pathogen and the hormonal environment of the human host, as suggested previously (*6*).

The number of proteins with which EBP1 shares sequence homology is steadily growing, and includes enzymes from both prokaryotic and eukaryotic sources (*7*−*12*). Perhaps the best known is Old Yellow Enzyme (OYE), a name given to several proteins of yeast origin that have been extensively studied since the discovery long ago (*13*) of what has turned out to be a mixture of isozymes in brewer's yeast. The thorough characterization of the OYE's (*14*) has provided a starting point for the examination of ligand binding and reactivity among subsequently identified homologues for which the physiological function is unknown, including EBP1.

Hallmark features of this family of flavoproteins include binding of ligands that contain a phenolic moiety and catalysis of reduction of the carbon−carbon double bond in compounds that contain an α,β-unsaturated ketone or aldehyde functionality with pyridine nucleotides as the source of electrons (*4, 9, 11, 12, 15, 16*). Both properties have been observed in every homologue in which they have been examined. However, the identity of the in vivo electron-accepting substrates for the OYE's and EBP1 remains uncertain.

Identification of a few homologues that have been isolated on the basis of a known catalytic activity has provided some clues for possible functions of the OYE's and EBP1. One

[†] This work was supported in part by grants to S.M.M. from the UCSF Academic Senate and the Charles E. Culpeper Foundation. J.B. was supported in part by an American Foundation for Pharmaceutical Education Fellowship and a University of California President's Dissertation Year Fellowship.

* To whom correspondence should be addressed. Email: smiller@cgl.ucsf.edu; tel: 415-476-7155; fax: 415-476-0688.

[1] Abbreviations: EBP1, estrogen binding protein; E_{ox}, oxidized EBP1; E_{red}, reduced EBP1; NADPH, nicotinamide adenine dinucleotide phosphate, reduced form; $NADP^+$, nicotinamide adenine dinucleotide phosphate, oxidized form; NADH, nicotinamide adenine dinucleotide, reduced form; NAD^+, nicotinamide adenine dinucleotide, oxidized form; HXL or hexenal, *trans*-2-hexenal; FMN, flavin mononucleotide; OYE, Old Yellow Enzyme; OPDA, 12-oxophytodienoic acid; RP-HPLC, reverse-phase high-performance liquid chromatography; CT, charge transfer; (K)IE, (kinetic) isotope effect; ATP, adenosine triphosphate.

10.1021/bi0006520 CCC: $19.00
Published on Web 08/04/2000

of the most intriguing of these is a homologue from the plant *Arabidopsis thaliana* that functions in a lipid signaling pathway. This homologue, OPDA reductase (OPR), functions in vivo to reduce the olefinic bond within a cyclopentenone moiety of 12-oxophytodienoic acid, one of the key lipids in the pathway (*11*). Moreover, in every eukaryotic homologue for which a physiological function has been identified, a pyridine nucleotide serves as reducing substrate and an α,β-unsaturated ketone serves as electron acceptor. While a signaling pathway of the sort identified in *Arabidopsis* has not been discovered in yeast, it is possible that such a pathway does exist, and EBP1 serves a function analogous to OPR. At the least, given the conservation of the reductase activity with α,β-unsaturated substrates in its homologues, it is likely that EBP1 acts upon a substrate(s) with the same functionality in vivo.

One approach that we are pursuing to identify the physiological substrate(s) is the design of mutants with altered catalytic properties that might be able to trap the electron-accepting substrate as an enzyme-bound intermediate. To identify suitable catalytically deficient mutants, we have undertaken a full characterization of the wild-type EBP1-catalyzed reduction of a model substrate, *trans*-2-hexenal, by NADPH. Previously, we have described several features of steady-state turnover with this and other substrates (*4*) and here extend the analysis to include pre-steady-state kinetic behavior. This study has allowed us to develop a more elaborate and comprehensive description of the microscopic kinetics and intermediates that occur along the reaction pathway. In addition, the analysis reveals an interesting facet of the kinetic isotope effects expressed in its course. These results may have broader implications in other studies of isotope effects within enzyme-catalyzed reactions, and extend the idea that these effects may occur intrinsically in the formation of protein·ligand complexes.

MATERIALS AND METHODS

Unless indicated otherwise, all reagents were the highest grade possible and obtained from Sigma Chemical. EBP1 was expressed and purified as described previously (*4*). All experiments described here were performed at 4 °C in 50 mM potassium phosphate buffer, pH 7.0.

Stopped-Flow Experiments. All rapid reaction studies were conducted using a HiTech SF-61DX2 instrument (Hi-Tech Ltd., Salisbury, U.K.). Data were collected as indicated in the text in either the single beam mode using photodiode array detection for simultaneous collection of spectral data, or the dual beam mode using photomultiplier detection for collection of either absorbance data at a single wavelength or fluorescence data. All except for the fluorescence quenching experiments were performed anaerobically. Protein samples were made anaerobic in a tonometer, designed and fitted for this type of work, by successive cycles of evacuation and reequilibration with oxygen-scrubbed argon. Other reagents were made anaerobic by bubbling with the same argon for at least 5 min. The instrument itself was made anaerobic by repeated filling and emptying of the drive syringes with an argon-bubbled solution of 10 mM glucose to which a catalytic amount of glucose oxidase was added. Catalase was also added in catalytic amounts to prevent the buildup of peroxide generated by the glucose/glucose oxidase system. The instrument was flushed in this manner until fresh, oxygen-free solution filled all portions of the flow path, and was prepared in this manner both the night before and the same morning that the experiments were performed.

For stopped-flow experiments with the reduced enzyme, the reagents were prepared as above and the enzyme was reduced in the tonometer using one of two methods. In the first procedure, used to study the reaction of reduced enzyme with $NADP^+$, sodium dithionite was dissolved in buffer, made anaerobic, and drawn into an airtight Hamilton syringe, which was fitted so that it can be attached to the cuvette without exposing either sample to air. Dithionite was added incrementally until the flavin cofactor was fully reduced by two electrons, as determined spectrophotometrically. The second procedure, used in studying the reaction of reduced enzyme with *trans*-2-hexenal, involved the inclusion of an NADPH-generating system, adopted from that described previously (*17*). Briefly, a solution of the enzyme, 4 mM glucose 6-phosphate, and 30 nM $NADP^+$ was made anaerobic as above, and a small amount (8 units) of glucose-6-phosphate dehydrogenase (G6PDH) was added subsequently. Under these conditions, i.e., very low concentrations of both pyridine nucleotide and G6PDH, reduction of EBP1 was complete in no less than 20 min, and, thus, this reaction does not interfere with the kinetics under study.

Equilibrium Titration of Reduced Enzyme with $NADP^+$. The protein sample was made anaerobic in a specially designed cuvette similar to those described previously and reduced by dithionite, as above. The syringe containing dithionite was then exchanged with one containing $NADP^+$ dissolved in buffer. The concentration of the $NADP^+$ stock solution was determined using an extinction coefficient of 18 000 M^{-1} cm^{-1} at 262 nm. The titration was performed at 4 °C, and spectra were recorded after each addition of $NADP^+$ using an HP8452 diode array UV−visible spectrophotometer (Hewlett-Packard).

Synthesis of β-[4(R)- and 4(S)-^{2}H]-NADPH. β-[4(*R*)-^{2}H]-NADPH was synthesized essentially according to the protocol developed by Ryerson et al. (*18*). Briefly, oxalacetic acid was reduced nonstereospecifically with sodium [^{2}H]-borohydride. The resulting deuterated malate was then used to generate stereospecifically labeled 4(*R*)-[^{2}H]-NADPH by reaction with malic enzyme. The labeled product was purified as described, followed by RP-HPLC using an analytical C18 column, with an increasing gradient of aqueous 0.2 M ammonium bicarbonate, pH 8.1, from 0 to 60% over 15 min. The absorbance was monitored at 260 and 340 nm, which indicated greater than 97% purity of the product by peak height (data not shown). Appropriate fractions were collected and pooled, quickly dried down at <40 °C in a rotary evaporator, and used either immediately or on the following day after storage at 4 °C overnight. β-[4(*S*)-^{2}H]-NADPH was synthesized as described (*19*), in a procedure originally designed to assay blood glucose levels. 1-[^{2}H]-Glucose (Cambridge Isotopes) was incubated with a solution of ATP and hexokinase. The resulting 1-[^{2}H]-glucose 6-phosphate was then used to transfer label stereospecifically via the enzymatic reduction of $NADP^+$ catalyzed by glucose-6-phosphate dehydrogenase. The product was purified and dried in the same fashion as the 4(*R*)-labeled diastereomer.

Data Presentation and Curve Fitting. Single-wavelength absorbance and fluorescence data were analyzed with the

Scheme 1

$$E_{ox} + NADPH \underset{k_2}{\overset{k_1}{\rightleftharpoons}} E_{ox}\cdot NADPH \underset{k_4}{\overset{k_3}{\rightleftharpoons}} E_{ox}\cdot NADPH^{*} \underset{k_6}{\overset{k_5}{\rightleftharpoons}} E_{red}\cdot NADP^{+} \underset{k_8}{\overset{k_7}{\rightleftharpoons}} E_{red} + NADP^{+}$$

Charge Transfer Complex

internal fitting component of the KinetAsyst software package (Hi-Tech Ltd.) that drives the instrument and data collection. Data were fit with models including a single or sum of exponential phases, as appropriate. In each case, the best fit was assigned as the simplest one giving the smallest deviation in a least-squares fit analysis and random residuals over the whole time course.

Time-resolved spectral data collected using diode array detection were analyzed using SPECFIT (Spectrum Software Associates, Chapel Hill, NC), a spectral analysis package that employs a singular value decomposition routine, global least-squares fitting, and factor analysis to calculate kinetic or equilibrium binding constants and corresponding spectral species for a given reaction.

All data shown, whether representative of true raw data or a derivative thereof were imported into and rendered by KaleidaGraph (Synergy Software). For each experiment not fit by either method mentioned above, the curve-fitting routine in KaleidaGraph was used to determine the fit with minimal least-squares deviation.

As will be elaborated under Results, the analytical expression for k_{obs} in the reoxidation by $NADP^+$ is derived from the reverse direction of the multi-equilibrium reaction path proposed in Scheme 1, where E_{ox} represents enzyme with fully oxidized FMN cofactor, the charge-transfer (CT) species is denoted with an asterisk, and E_{red} represents enzyme with 2-electron-reduced FMN cofactor. Since the fluorescence quench experiment described below indicates very tight binding and slow dissociation of NADPH to oxidized enzyme, this step was not included in the analysis of the back-reaction. Thus, the analytical form for the observed rate constant for reoxidation of E_{red} by $NADP^+$ includes the constants involved in binding (k_7 and k_8), the equilibrium formation of the CT complex (k_5 and k_6), and the subsequent equilibration of this and the E_{ox}·NADPH Michaelis complex (k_3 and k_4).

A solution for the rate constant (k_{obs}) governing formation of the E_{ox}·NADPH complex from $E_{red} + NADP^+$ (Scheme 1, reverse direction) was derived using a slightly modified version (*20*) of the steady-state approach described by Strickland et al. (*21*). For this approach, the E_{red}·$NADP^+$ and E_{ox}·NADPH* complexes were assumed to be in steady-state, and the kinetic expression was assumed to include terms only up to the E_{ox}·NADPH Michaelis complex, as explained above. Furthermore, oxidized enzyme, which gives rise to the signal being measured, is represented in both complexes with the reduced pyridine nucleotide. Because the expression was originally derived for the formation of the final species in the reaction, in this case the E_{ox}·NADPH Michaelis complex, we have also made the tacit assumption that the formation of the CT complex occurs at about the same rate, i.e., is rate-limiting in formation of both oxidized enzyme complexes. This assumption holds at the end of the analysis, where the sum of the constants for the formation of the CT complex is much smaller (>15-fold) than that for the formation of the Michaelis complex. In summary, the derivation of the analytical expression is dependent on simplifying assumptions that may not describe the reaction as it truly occurs, but nonetheless results in values that correspond reasonably well with those obtained by different means (see below). In this case, the observed rate constant for the formation of E_{ox} in its complexes with NADPH is given by eq 1:

$$k_{obs} = (k_1k_3k_5 + k_1k_4k_6 + k_1k_3k_6)[NADP^+] - k_5k_6(k_2 + k_3) + k_6[(k_4 + k_5)(k_2 + k_3) - k_3k_4]/(k_1k_3 + k_1k_4 + k_1k_5)[NADP^+] + (k_4 + k_5)(k_2 + k_3) - k_3k_4 \quad (1)$$

Kinetic Simulations. Single-wavelength stopped-flow data were exported from the KinetAsyst software as text files, and a deadtime of 1.54 ms, experimentally determined according to the manufacturer's protocol, was added to all time points. Models were constructed for KINSIM (*22*, *23*) that represent the reductive half-reaction, Scheme 1, in either the forward or the reverse direction, as appropriate.

Estimates and constraints for the values of the intrinsic rate constants for simulating the reductive reaction in the forward direction were assembled from the values of the observed rate constants and the fluorescence quench data. Estimates for fits to the reaction in the backward direction were compiled from the values obtained from the fit to the observed rate constant in the reaction of E_{red} with $NADP^+$ and the value of the apparent dissociation constant for the E_{red}·$NADP^+$ complex, obtained by titration of E_{red} with $NADP^+$. Since this reaction proceeds to an equilibrium mixture of E_{ox}·NADPH and E_{ox}·NADPH*, the expression for the apparent dissociation constant is given by eq 2:

$$K_{d(app)} = \frac{K_1K_2K_3}{1 + K_2K_3 + K_3} \quad (2)$$

where $K_1 = k_7/k_8$, $K_2 = k_5/k_6$, and $K_3 = k_3/k_4$.

To reproduce the raw absorbance data, values of the extinction coefficients for all species at the wavelengths studied were estimated based on values for similar species in other enzymes described in the literature, the results of other experiments not necessarily included here, and/or reasonable approximations based on the observed behavior in the diode array experiments. For instance, the extinction coefficient of the CT complex at 550 nm was evaluated from the value of the maximum absorbance at this wavelength during the reaction relative to that in the initial and final spectra, knowledge of coefficients of other charge-transfer species with this enzyme, and the estimated value of the microscopic equilibrium constant between this and the initial binary complex. Values for this and the other relevant species are indicated in the figure legends for each experiment. Iterative cycles of simulation, varying extinction coefficients and rate constants, and refining the values put into the curve

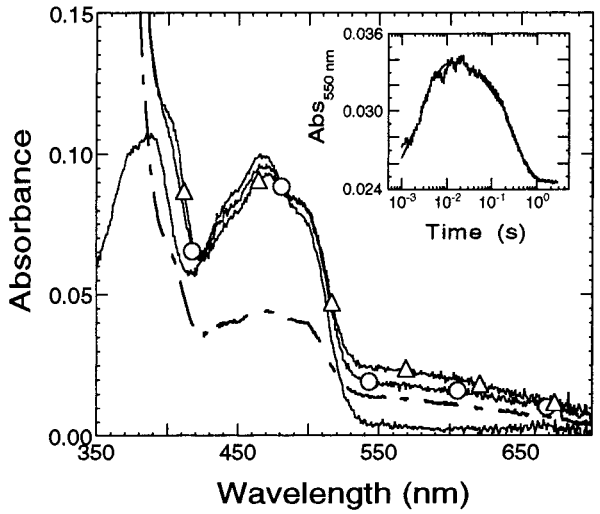

FIGURE 1: Reduction of EBP1 with NADPH. (A) UV−visible spectra collected in the diode array mode during rapid reduction of 10.7 μM EBP1 with 82 μM NADPH. Spectra were recorded at 4 (○), 11 (△), and 7125 ms (dashed line) after mixing. The spectrum of E_{ox} (solid line) was obtained from a different shot of enzyme against buffer and is included to illustrate the extensive development of charge transfer in the first spectrum collected at 4 ms. Inset: Semilogarithmic plot of data collected at 550 nm in the single-wavelength mode with identical reagent concentrations as in the main panel. Data are overlaid with fit to biphasic exponential process, giving observed rate constants of 355 ± 6 and 3.30 ± 0.03 s^{-1}, respectively.

fits, were carried out until sets of values were obtained that reproduced all data sets satisfactorily.

RESULTS

Reductive Half-Reaction with NADPH. Pyridine nucleotides, NADPH and/or NADH, are the typical reducing substrates of the enzyme-bound FMN in this family of proteins (*4*, *9*, *11*, *13*, *16*, *24*). We have shown that EBP1 exhibits a strong preference for NADPH in steady-state reactions, as do a number of the other homologues. To examine the reaction in more detail, we have evaluated the reduction of the enzyme in the stopped flow.

Figure 1 depicts a typical experiment performed in the diode array absorbance mode in which the oxidized enzyme is combined anaerobically with NADPH. Primary inspection of the data reveals that the reaction can be modeled as a simple irreversible biphasic process described by the sum of two exponentials with broad changes to the absorption spectrum of the flavin occurring in a fast phase followed by further changes in a slow phase. The first phase, which progresses substantially within the deadtime, is characterized by a slight decrease in the absorbance of the main flavin band at 466 nm and increases in absorbance both in the 405 nm and in the long-wavelength regions. These spectral features are characteristic of the formation of a charge-transfer complex between NADPH and enzyme-bound FMN. As described previously (*25*), the absorbance properties of this complex are due to the transfer of an electron from a donor orbital of the pyridine nucleotide to an acceptor orbital of the electron-deficient isoalloxazine ring of the flavin upon excitation by light of an appropriate wavelength. Formation of such a CT complex implies a very specific spatial and electronic orientation of the molecules involved, and its presence in the reaction pathway might be understood as the preparation of the reactants for electron transfer.

The slower phase is characterized by a decrease of absorbance in the flavin main band and in the long-wavelength band, consistent with the transfer of a hydride equivalent from bound NADPH to FMN resulting in formation of an E_{red}•$NADP^+$ complex. The final spectrum in the reaction, which was invariant with NADPH concentration, clearly retains some of the oxidized enzyme intermediate, indicating that the reaction is a reversible equilibrium process.

While data collection in the diode array mode provides an advantage with respect to observation of broad spectral features and species assignment, the 1.5 ms resolution of the data limits the accuracy in the determination of very fast processes. Therefore, to examine the first phase more carefully and to investigate the effect of substrate concentration, data were collected using the photomultiplier mode of the instrument. The reaction was monitored at 405 and 550 nm to follow the formation and decay of the CT intermediate, and at 487 nm, an isosbestic for the first two apparent species identified in the diode array analysis, to monitor flavin reduction explicitly.

The inset to Figure 1 depicts a representative data trace collected at 550 nm. The biphasic, "up−down" behavior is readily apparent, and data analysis using an A → B → C model yields values for the observed fast and slow rate constants of 355 ± 6 and 3.30 ± 0.03 s^{-1}, corresponding to charge-transfer development and decay, respectively. Traces collected at 405 nm, which also exhibit up−down behavior, were well fit to the same values as those for corresponding data at 550 nm. As expected from the diode array data, the 487 nm transient is monophasic and yields a rate constant for the slow phase that closely matched that for the other wavelengths. The magnitudes of both observed rate constants are essentially constant at all experimentally accessible concentrations of NADPH (i.e., high enough to maintain pseudo-first-order conditions) (data not shown). The lack of a concentration dependence in the formation of the CT complex indicates that binding of NADPH occurs in a step preceding the transient leading to formation of the CT absorbance. In addition, binding is fully saturated under all conditions examined and is complete within the deadtime of the instrument. The minimal mechanism consistent with these observations is given in Scheme 1, where the transients observed in the visible spectra are representative of equilibrium conversion of the E_{ox}•NADPH complex to the CT complex and equilibrium conversion of the CT complex to the combined reduced enzyme species. A similar scheme has been reported for the reaction of OYE with pyridine nucleotides (*26*).

To verify that binding of NADPH occurs more rapidly than is observable in the UV−visible absorbance mode, we examined the kinetics of quenching of NADPH fluorescence using a low, constant concentration of NADPH and a variable excess of EBP1. Although loss of fluorescence occurs upon oxidation of NADPH, fluorescence quenching also frequently occurs simply upon binding to flavoenzymes [e.g., to the EH_2 form of disulfide reductases(*27*)], and the magnitude and concentration dependence of the observed rate constant for quenching allow distinction between the two possibilities. As depicted in Figure 2, the observed rate constant for the quenching reaction is linearly dependent on the concentration

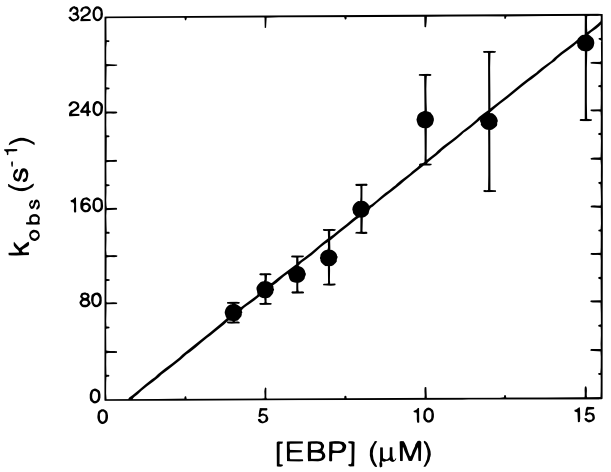

FIGURE 2: Dependence of the observed rate constant for quenching of 0.5 μM NADPH fluorescence on the concentration of EBP1. The line was generated from a weighted least-squares fit to the data as described in the text. The value of the rate constant for association of E_{ox} and NADPH is given by the slope, $k_{on} = (2.1 \pm 0.3) \times 10^7$ M^{-1} s^{-1}. The rate constant for dissociation of NADPH is given by the *y*-intercept (-15 ± 17 s^{-1}, interpreted as a maximal $k_{off} = 1$ s^{-1}, see text). The same experimental procedure using the *pro-R* deuterated isotopomer resulted in a value for k_{on} of $(2.5 \pm 0.6) \times 10^7$ M^{-1} s^{-1} (data not shown).

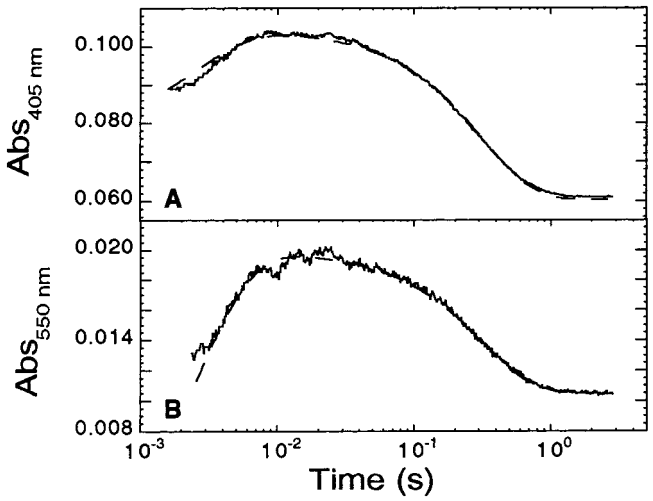

FIGURE 3: Simulation of data from reduction of EBP1 with NADPH. Data traces (solid lines) collected from two separate experiments at (A) 405 nm and (B) 550 nm during reduction of EBP1 with NADPH under conditions identical to those given in the inset to Figure 1. The data are overlaid with simulated data (dashed lines) using the model of Scheme 1, substituting the values for each microscopic rate constant with that given in the first column of Table 1. In (A), the following extinction coefficients for each species were determined or estimated as described in the text: $\epsilon_{405}(E_{ox}) = \epsilon_{405}(E_{ox}{\cdot}NADPH) = 7550$ M^{-1} cm^{-1}, $\epsilon_{405}(E_{ox}{\cdot}NADPH^*) = 11\,200$ M^{-1} cm^{-1}, and $\epsilon_{405}(E_{red}{\cdot}NADP^+) = \epsilon_{405}(E_{red}) = 1550$ M^{-1} cm^{-1}. In (B), the following extinction coefficients were used: $\epsilon_{550}(E_{ox}) = \epsilon_{550}(E_{ox}{\cdot}NADPH) = 0$ M^{-1} cm^{-1}, $\epsilon_{550}(E_{ox}{\cdot}NADPH^*) = 3100$ M^{-1} cm^{-1}, and $\epsilon_{550}(E_{red}{\cdot}NADP^+) = \epsilon_{550}(E_{red}) = 100$ M^{-1} cm^{-1}.

of enzyme used, indicating that the process observed is second order and represents the combination of enzyme and substrate. The association rate constant, k_1, is obtained from the slope of the line, resulting in a value of $(2.1 \pm 0.3) \times 10^7$ M^{-1} s^{-1}. This yields a pseudo-first-order rate constant of $\sim$1600 s^{-1} under the conditions of the absorbance mode experiments, confirming that binding is indeed complete within the deadtime of those experiments. The dissociation rate constant, k_2, obtained from the *y*-intercept (*28*), is apparently too small compared to the observed rates to be determined reliably under these conditions: the linear fit using standard errors to weight each data point extrapolates to a negative value at the *y*-axis (-15 ± 17 s^{-1}). While there is no physical significance of a negative *y*-intercept value, it is possible to obtain such a result within the error observed in these measurements. Thus, for the simulations described below, we set the value of k_2 at 1 s^{-1} and a corresponding value for the equilibrium dissociation constant, K_d, of 50 nM.

Simulation of the UV−visible absorbance traces was performed using the model in Scheme 1. The values of the observed rate constants in the absorbance data and those for k_1 and k_2 obtained from the fluorescence quench experiment were used as a basis for estimating the microscopic rate constants. Figure 3 shows an overlay of simulations with the raw data shown in the inset of Figure 1 and another trace collected in a separate experiment at another wavelength. Clearly, the traces can be simulated using the values given in Table 1 with very good agreement to the actual data.

To verify that the rate constants obtained in the simulation accurately represent the reaction, the half-reaction in the reverse direction was examined. In accord with the principle of microscopic reversibility, the process in this direction should be faithfully represented with the same constants used in the forward direction. In these experiments, reduced enzyme was generated by titration with dithionite and combined with $NADP^+$ anaerobically in the stopped flow. The reaction with varied concentrations of $NADP^+$ was monitored at 466 nm, and resulted in a monophasic increase in absorbance, indicating that reoxidation of the flavin occurs in a single-exponential phase (data not shown). As shown in Figure 4A, the observed rate constant for the process exhibits a saturating dependence on the concentration of $NADP^+$. This behavior is consistent with the formation of an $E_{red}{\cdot}NADP^+$ complex followed by transfer of a hydride equivalent from reduced flavin to bound $NADP^+$, resulting in formation of an equilibrium mixture of the $E_{ox}{\cdot}NADPH^*$ CT and $E_{ox}{\cdot}NADPH$ Michaelis complexes, as indicated in Scheme 1 (*21*). Since both of these complexes give rise to the oxidized flavin signal, the observation of only a single transient indicates that the rate-limiting step after binding of $NADP^+$ is the hydride transfer to form the CT complex and any subsequent equilibration to the Michaelis complex occurs more rapidly. This is consistent with the spectral

Table 1: Microscopic Rate Constants for the Reduction of EBP1 with NADPH and β-[4(*R*)-^{2}H]-NADPH

constants	from simulation[a]	experimental[b]	with β-[4(*R*)-^{2}H]-NADPH[c]
k_1	2×10^7 M^{-1} s^{-1}	$(2.1 \pm 0.3) \times 10^7$ M^{-1} s^{-1}	$(2.5 \pm 0.6) \times 10^7$ M^{-1} s^{-1}
k_2	1 s^{-1}	not determined	1 s^{-1}
k_3	250 s^{-1}	220 s^{-1}	86 s^{-1}
k_4	165 s^{-1}	187 s^{-1}	60 s^{-1}
k_5	2.4 s^{-1}	8 s^{-1}	1.55 s^{-1}
k_6	24 s^{-1}	26 s^{-1}	5.5 s^{-1}
k_7/k_8	8×10^{-5} M	2.1×10^{-3} M	8×10^{-5} M

[a] Determined from overlay of raw and simulated data for reactions monitored at 405, 487, and 550 nm (see Figure 3). [b] k_1 determined from fit to data of Figure 2, all others from fit to data of Figure 4A (see text). [c] Determined from overlay of raw and simulated data for reactions monitored at 550 nm.

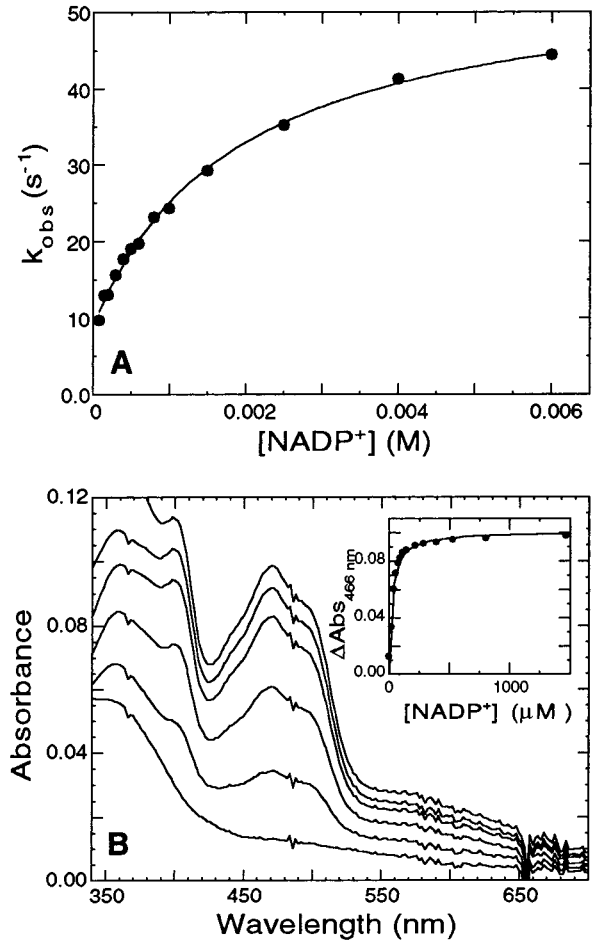

FIGURE 4: Reoxidation of reduced EBP1 with $NADP^+$. (A) Observed rate constant for reoxidation of reduced EBP1 with increasing concentrations of $NADP^+$. The curve is that obtained from the fit of the data to eq 1, yielding values presented in the second column of Table 1. (B) UV−visible spectra accompanying titration of 9.2 μM dithionite-reduced EBP1 with $NADP^+$. Final concentrations in order of increasing absorbance: 0, 17.9, 35.8, 89.4, 213.7, and 1463.4 μM. Inset: Absorbance changes at 466 nm resulting from addition of $NADP^+$. The curve represents the least-squares fit to a hyperbolic expression that gives an apparent K_d for the E_{red}·$NADP^+$ complex of 29 μM, the same value calculated from substitution of the kinetic constants obtained in the fit to the data in (A) into eq 2.

changes associated with the fast and slow phases in the forward direction, where equilibrium formation of the CT complex occurs ~100× more rapidly than the hydride transfer step. A good fit to the expression for k_{obs} given by eq 1 was obtained with initial estimates based on the simulations of the forward half-reaction to give the values listed in the second column of Table 1. Furthermore, the rate constants obtained from fitting the overall dependence of k_{obs} on [$NADP^+$] provide a good fit when used to simulate the individual data traces from the experiments at each reagent concentration (data not shown).

In theory, it should be possible to extract information from the dependence of the amplitude on $NADP^+$ concentration as well, but there was surprisingly little variation in these data. This was better understood after an equilibrium titration of dithionite-reduced enzyme with $NADP^+$ was carried out. As shown in Figure 4B, the reaction is almost fully reversible. That is, a sufficient concentration of $NADP^+$ can drive the enzyme back to a species that appears to be largely the E_{ox}·NADPH* complex. Though there is some uncertainty with regard to the extinction coefficients of the species involved, the fact that the final spectrum displays substantial long-wavelength absorbance further attests to the tight binding of NADPH to E_{ox}, and an equilibrium favoring the CT complex over the initial E_{ox}·NADPH Michaelis complex. A simple hyperbolic fit to the titration data (Figure 4B, inset) results in an apparent dissociation constant of 29 ± 4 μM for the "E_{red}·$NADP^+$" complex. Thus, the limited dependence of amplitude in the kinetic experiments is explained by the fact that the lowest concentration of $NADP^+$ necessary to obtain the pseudo-first-order condition in the kinetics (80 μM), more than 2.5-fold over the $K_{d(app)}$, was approaching "saturation" of the reduced enzyme with regard to the final amount of reoxidation. Examination of the factors that comprise $K_{d(app)}$ (eq 2) reveals that it is the back-reaction of the chemical step, that is, transfer of hydride from the reduced flavin to $NADP^+$, that pulls the overall equilibrium and causes the apparent dissociation constant to be much smaller (tighter) than the true value.

Comparison of the first and second columns of Table 1 reveals that the values from simulation of the forward reaction versus those from the fit to the back reaction agree reasonably well, except perhaps for those given for the true K_d (k_7/k_8) of the E_{red}·$NADP^+$ complex, and, hence, the expected apparent K_d. It is noteworthy that the value for $K_{d(app)}$, calculated from the kinetic data for the back-reaction (29 μM) is identical to that obtained from the equilibrium titration involving the same reactants (see Discussion).

We do not claim that the set of kinetic constants given for the reductive half-reaction in the forward direction represents a unique solution for this system, but it does provide a framework within which to examine analogous data with isotopically labeled compounds (see below) and is self-consistent thermodynamically:

From Scheme 1, the apparent dissociation constant for oxidized enzyme and NADPH is given by

$$K_{d(app)} = \frac{[E_{ox}][NADPH]}{[E_{ox}\cdot NADPH] + [E_{ox}\cdot NADPH^*]} = \frac{k_2/k_1}{1 + k_3/k_4} = 20\ \text{nM} \quad (3)$$

while the value for the dissociation constant for the reduced enzyme and $NADP^+$ is

$$K_d = \frac{[E_{red}][NADP^+]}{[E_{red}\cdot NADP^+]} = \frac{k_7}{k_8} = 80\ \mu\text{M} \quad (4)$$

Thus, the enzyme binds the pyridine nucleotide cofactor 4000 times tighter in its reduced than in its oxidized state. This results in an increase in the reduction potential relative to the unbound state, and corresponds to a change in the midpoint potential for the bound NADPH of 108 mV [~30 mV(log 4000)]. Thus, the midpoint potential of NADPH is raised to a value of −212 mV, 34 mV more positive than that for the FMN on the enzyme, −246 mV (*4*). One would expect, then, that the internal equilibrium for electron transfer described by the constants k_5/k_6 should favor the oxidized enzyme by about 10 to 1, which is consistent with the constants obtained from simulation.

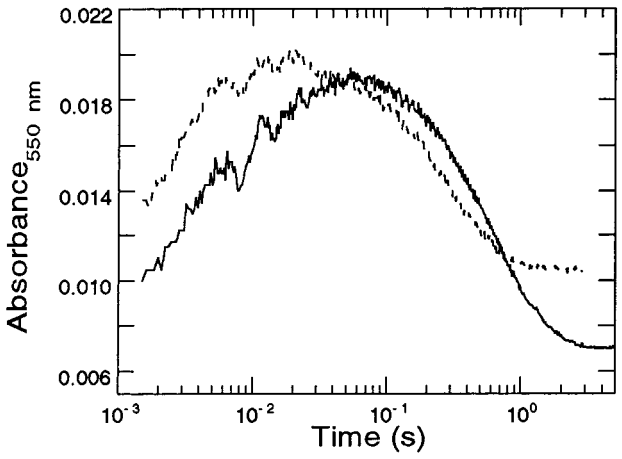

FIGURE 5: Reduction of EBP1 with β-[4(*R*)-^{2}H]NADPH. Semilogarithmic plot of absorbance trace collected at 550 nm in the stopped flow with 4(*R*)-[^{2}H]- and 4(*R*)-[^{1}H]-NADPH, represented by the solid line and the dashed line, respectively. The two traces were collected using identical reagent concentrations, and are the same as given for the inset to Figure 1.

Isotope Effects with β-[4(R)-^{2}H]- and β-[4(S)-^{2}H]-NADPH. The effect on the kinetics of the reductive half-reaction was evaluated using NADPH that was stereospecifically deuterated in either the *pro-R* or the *pro-S* position, to determine the stereospecificity of hydride transfer in this system. The reaction was qualitatively similar with either diastereomer, as examined in the diode array mode (data not shown), and proceeded in a biphasic fashion, like that described above. Comparison of the phases in the reaction with *pro-S* deuterated versus protio-NADPH shows small differences in both phases, but the magnitudes are too small to quantitate the effect reliably (data not shown). However, the reaction with deuterium in the *pro-R* position gives some unexpected results.

Data were collected using [4(*R*)-^{2}H]-NADPH in the photomultiplier mode at 550 nm in the same fashion as that for the protio-NADPH. Figure 5 illustrates a typical data trace overlaid with data for the protio isotopomer for comparison. It is apparent that the amplitudes are different in the two reactions, with the fast phase progressing slightly less with the deuterio than with the protio isotopomer. The slow phase, in contrast, progresses further, indicating an effect on the equilibrium for the chemical step that favors reduction of the enzyme. Both observed rate constants are again independent of NADPH concentration (data not shown). Surprisingly, both observed rate constants exhibit a fairly significant isotope effect, a 4.7-fold and 2.2-fold k_{Hobs}/k_{Dobs} effect on the fast and slow phases, respectively. So at first glance, there appears to be a more pronounced effect on the step that is thought to precede bond cleavage than the cleavage step itself! It occurred to us that the decreased rate of the first phase might be caused by the presence of some inhibitor present in the deuterated material that was not removed during purification. Therefore, protio-NADPH was synthesized in the same fashion, and similar results were obtained as with the commercial preparation. Furthermore, results of a fluorescence quench experiment with the deuterated material like that described above in Figure 2 clearly showed that there was no significant effect on the association rate using the *pro-R* deuterio isotopomer (data not shown).

The phenomenon in which isotope effects are observed in steps that occur proximate to the bond cleavage step is one that has been characterized and revisited, and is usually explained by a similarity in the rates of the isotopically sensitive and insensitive steps (*28*−*30*). However, the apparent rate constants that characterize the reactions studied here differ by a factor of greater than 100 for the protio isotopomer and greater than 70 for the deuterio isotopomer. With a factor this large, and if the apparent rates reflect only the intrinsic microscopic rates for each step, they should be well resolved and "kinetic mixing" would not be expected. Still, we explored models in simulation in which this was not the case; i.e., the magnitude of one of the rates in the bond cleavage step (k_6) was set so that the sum of the forward and backward rates ($k_5 + k_6$) was comparable to that of CT formation ($k_3 + k_4$). Although a reasonable fit could be obtained with values that satisfied this condition, the resulting k_4 was >150 times the value of k_3, somewhat implausible chemically, and the values of the on-enzyme vs off-enzyme reduction potentials do not "balance", as laid out above. Furthermore, and most importantly, under no numerical conditions sampled could a good fit be obtained without including some isotope effect on the CT formation step.

Further support for this conclusion is given by a treatment of the data suggested in a recent monograph by Fisher and Saha (*31*). They suggest that isotope effects in transient-state kinetic data should be treated similarly to those in steady-state; that is, the kinetic isotope effect (KIE) is one on the rate itself, as opposed to the effect on the observed rate constants as described above. In that paper, simulations were presented showing the effect on the ratio of the rates of change of a measured signal with respect to time (dS/dt) for reactants in a system where deuterium is substituted for protium in a bond cleaved during the reaction. Systems that involve multiple sequential equilibria like that described here were considered, and the impact on the KIE_{obs} [defined as $(dS/dt)_H/(dS/dt)_D$] vs time was evaluated when the signal resulted from species that occur only before, only after, or both before and after the isotopically sensitive step. The results of such simulations led to the general conclusions that when only the species appearing after an isotopically sensitive step contributes to the observed signal, the observed KIE will equal the intrinsic KIE for that step at $t = 0$, and will decrease with time. In contrast, if the species that generates the signal occurs before the isotopically sensitive step, the KIE_{obs} will equal 1 at $t = 0$ and then decrease with time. In the fast phase of our reaction, the signal is the appearance of the long-wavelength band attributable to the CT complex. In Figure 6, the data are presented in the form suggested by Fisher and Saha, and it is clear that the KIE_{obs} is almost 4 at $t = 0$, suggesting that the first case is true; that is, the CT complex is preceded by an isotopically sensitive step, namely, its formation.

Reoxidation with trans-2-Hexenal. Although the physiological electron acceptor has not yet been identified for EBP1, this protein shares the ability with other OYE family enzymes to reduce the olefinic bond of a variety of α,β-unsaturated carbonyl substrates. *trans*-2-Hexenal was chosen as a model oxidant for its desirable properties of a relatively low K_m, high turnover rate, and simple, saturating steady-state behavior (*4*). The spectral features in the reoxidation of reduced enzyme by hexenal are illustrated in Figure 7,

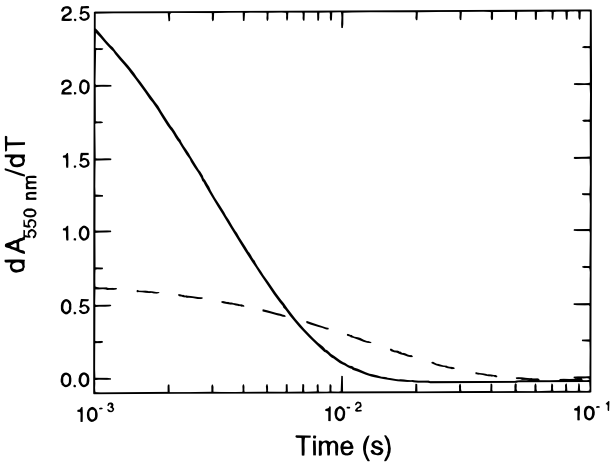

FIGURE 6: Velocity of reduction of EBP1 with β-[4(*R*)-^{1}H]NADPH (solid line) and β-[4(*R*)-^{2}H]NADPH (dashed line). As described in the text, the KIE may be expressed as the ratio of the two velocities, a value of ~4 at 1 ms, the earliest reliable data point collected after mixing. Curves shown are derivatives of the data traces of Figure 5 after applying the smoothing function within KaleidaGraph to the raw data for the sake of clarity of presentation.

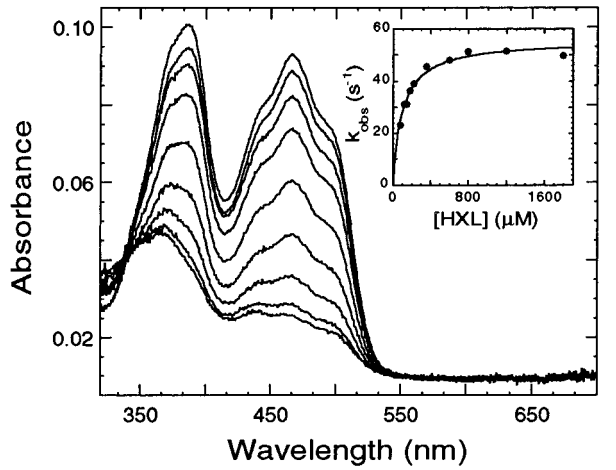

FIGURE 7: Reoxidation of reduced EBP1 with *trans*-2-hexenal. UV−visible spectra collected in the diode array mode of the stopped-flow instrument 3, 7, 17, 35, 66, 110, 154, 256, and 1900 ms (in order of increasing absorbance) after mixing 9.53 μM reduced EBP1 with 100 μM hexenal (final concentrations). Enzyme was reduced immediately before the experiment with the NADPH-generating system described under Materials and Methods. Inset: Observed rate constant obtained from a series of experiments at increasing concentrations of hexenal, using data collected at 466 nm in the photomultiplier mode. The curve represents the least-squares fit to the hyperbolic expression as described in text, yielding a value for k_3 of 56 ± 1 s^{-1} and a dissociation constant for the E_{red}·hexenal complex, k_2/k_1, of 100 ± 9 μM, as presented in Scheme 2.

the results of a typical stopped-flow experiment. In contrast to the NADP$^+$ reoxidation experiments described above, the enzyme used for these studies was reduced with an NADPH-generating system, described under Materials and Methods. The kinetics of reoxidation appear to be straightforward, and analysis of the data with SPECFIT reveals a good fit to a single-exponential process. The value of the observed rate constant varies hyperbolically with the concentration of substrate (Figure 7, inset). This behavior indicates that the reoxidation is preceded by a saturable equilibrium, most simply interpreted as the binding of HXL to the reduced enzyme (*21*), as presented in Scheme 2. The dissociation

Scheme 2

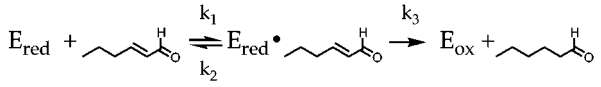

constant for the E_{red}·HXL complex resulting from this analysis is equal to the concentration of substrate required for the half-maximal rate constant, K_d = 100 ± 9 μM. Furthermore, in the simplest interpretation based on Scheme 2,[2] the intrinsic rate constant for the chemical step is obtained from the asymptote approached at infinite substrate concentration, when the reaction is limited by that step alone. Finally, the data are well fit to an expression that describes a rectangular hyperbola that intersects the *y*-axis at the origin, consistent with reduction of the substrate by the enzyme being irreversible. This conclusion is supported by results of experiments in which anaerobic titration of oxidized enzyme with hexanal led to very weak binding (K_d ~ 2 mM), but no reduction of enzyme flavin (data not shown).

In clear contrast to the reoxidation of the enzyme with NADP$^+$, the final species that obtains on reoxidation with hexenal does not contain the characteristic long-wavelength absorbance of a charge-transfer complex. However, the absorption spectrum does not appear to correspond exactly with that of free oxidized enzyme. Specifically, it appears that the peak centered at 385 nm has an increased extinction at the expense of the longer wavelength band centered at 466 nm. It also does not resemble the endpoint species in titrations of oxidized enzyme with the product, hexanal, which exhibits only minor perturbations of the flavin spectrum that are different from those observed here, and would not be expected to form to a significant extent given the weak binding mentioned above.

The final species at the end of reactions of the reduced enzyme with other α,β-unsaturated ketones, including cyclohexenone and nortestosterone, are similar in appearance, so this cannot be the result of an artefactual reaction with the aldehyde. In fact, we noted this behavior previously using nortestosterone as substrate (*4*), and postulated that the steroid stabilized the anionic semiquinone of the flavin cofactor somehow, because of the increased absorbance at 380 nm relative to the longer wavelength absorbance band. This is a characteristic feature of FMN in this (anionic semiquinone) state on OYE (*32*), among other proteins. If this was the case, we might expect exposure to oxygen to return the protein, if even at a very small rate, to the fully oxidized level. However, experiments in which the completed reaction of E_{red} and a stoichiometric amount of HXL was allowed to sit exposed to air overnight did not result in the return of the "normal", i.e., free E_{ox} spectrum (data not shown).

Adducts at the C4a position of the flavin often have increased absorbance in this same region, with greatly reduced absorbance in the other, longer wavelength main band (*33*), so we explored the possibility that this spectrum

[2] The data presented here are consistent with the minimal mechanism given in Scheme 2. However, as will be discussed in the following paper (*42*), the mechanism is probably more complex, involving another intermediate that is not visible in the reaction with wild-type enzyme. In this case, the saturated rate of "reoxidation" observed here is likely to reflect the intrinsic rate of formation of this intermediate, and the true rate of reoxidation is so much faster that the intermediate does not accumulate to a significant amount.

Scheme 3

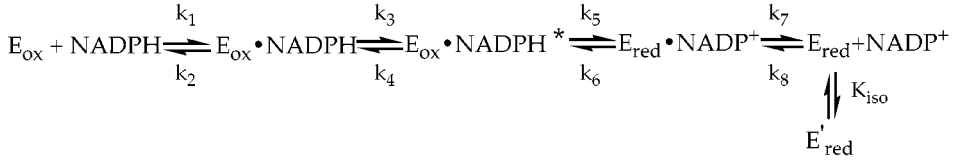

represents some small amount of a C4a-adduct that forms along with primarily free E_{ox}. Thus, the completed reoxidation reaction mixture that had been exposed overnight to air was then concentrated in a centrifugal filtration device and resuspended with no effect on the spectrum. The resuspended reaction was then returned to the filtration device, concentrated, and washed with buffer several times and resuspended, again, with no effect. While reversible adduct formation would not be expected to remain stable after successive washes, the results of several multiple turnover experiments do not support irreversible adduct formation, where one would expect to observe ever greater amounts of this adduct formed with increasing amounts of turnover. Further experiments are required to identify the nature of this unusual species. It is interesting that a spectrum with very similar properties seems to result from the reaction of the reduced EBP1 homologue, morphinone reductase, and its substrate, codeinone (*34*). This, therefore, may be a more general property of the reoxidation reactions catalyzed by this family of flavoproteins.

DISCUSSION

It is clear from these results that NADPH serves well as a reductant of the enzyme, and previous studies indicated the substantial discrimination between this cofactor and NADH in steady-state turnover. Though it cannot be rigorously excluded that another reductant might function in vivo, the extremely tight binding demonstrated here and the propensity of the enzyme to interact strongly with aromatic ligands in general suggest that NADPH is indeed the functional electron donor. Other homologues of EBP1, the OYE's, OPDA reductase, and pentaerythritol tetranitrate reductase, are also believed to use NADPH as substrate (*9*, *11*, *26*).

The complexity of the multi-equilibrium sequence in the reductive half-reaction and the limitations on the system experimentally prevented direct determination of each of the microscopic rate constants involved. However, the consistency of the rate constants reported here, evaluated from many different types and repetitions of experiments, to explain and reproduce the data sets lends credibility to the results. The only major discrepancy in the data exists between the value for the apparent dissociation constant of the E_{red}•$NADP^+$ complex, which appears to be ~5 μM in the results from data collected in the forward direction but 29 μM from data collected in the reverse. Though these values do not seem to be very different, their reproducibility, especially as derived from completely different experiments on different instruments (cf. transient kinetics and equilibrium titration), suggests that there may be a physical basis. One trivial explanation is that the value of 5 μM derived from the forward reaction comes from simulations with estimates for extinction coefficients that are inherently inexact. However, attempts to alter the coefficients and rate constants to give a value for $K_{d(app)}$ of 29 μM resulted in coefficients that were unrealistic and disagreed with results of previous work. Furthermore, the good agreement of the fits using the same rate constants at different wavelengths, which involved independent estimation of extinction values, argues against this possibility. It is also possible that the values obtained from the fit of the k_{obs} vs $NADP^+$ plot (Figure 4A, second column in Table 1) are in error because the expression for k_{obs} is oversimplified and incorrect (see Materials and Methods). However, again, the fact that the same result for $K_{d(app)}$ was obtained from the titration suggests that the expression for k_{obs} is reasonably accurate. Another possibility that would reconcile the discrepancy without altering any of the parameters reported here is that there is something fundamentally different about the two reactions as studied in the opposite directions. One difference we can identify is the need to artificially generate reduced enzyme to study the reverse reaction. In the forward direction, reduced enzyme is generated only by hydride transfer from NADPH. In contrast, for both studies of the reverse reaction with $NADP^+$, the enzyme was reduced with dithionite. It is feasible that reduction with dithionite leads to formation of an enzyme form that is largely unable to bind $NADP^+$ (Scheme 3). The results in the forward and reverse direction can be made to agree if one assumes a value for K_{iso} of 5.4 that favors the very low or no affinity state.

Perhaps the most controversial aspect of the results presented here is the observation of an isotope effect on the formation of the charge-transfer species that occurs before and in preparation of hydride transfer. Traditionally, isotope effects of the magnitude observed here have been associated with a bond cleavage event alone. However, the presence of an isotope effect upon binding of labeled ligands to various enzymes is not unprecedented. Effects have been reported for binding of [4-^{2}H]-NAD^+ to lactate dehydrogenase (*35*), of [4-^{2}H]-NADH to alcohol dehydrogenase (*36*), and of [^{18}O]-pyruvate to pyruvate decarboxylase and pyruvate kinase (*37*). These studies demonstrated a range of effects (a normal effect of 1.10 with lactate dehydrogenase, and an inverse effect of 0.52 with alcohol dehydrogenase) on the dissociation constants for complexes of the deuterated ligands and their macromolecular targets. Explanations offered for these isotope effects include differential solvation of the isotopomers, changes in vibrational and/or stretching frequencies of the isotopically substituted bond upon binding, and a difference in the charge on the atoms resulting from a change in the polarization of the bond relative to the unbound state that alters the bond-stretching force constant. On this last point, Cook et al. have indicated that deformation of the pyridine ring of the nicotinamide cofactor leads to increased carbocation character at C4 (*38*). LaReau et al. subsequently reasoned that the binding of NAD^+ to lactate dehydrogenase may very well induce strain and/or deform the molecule in this manner so that the increase of carbocation character and

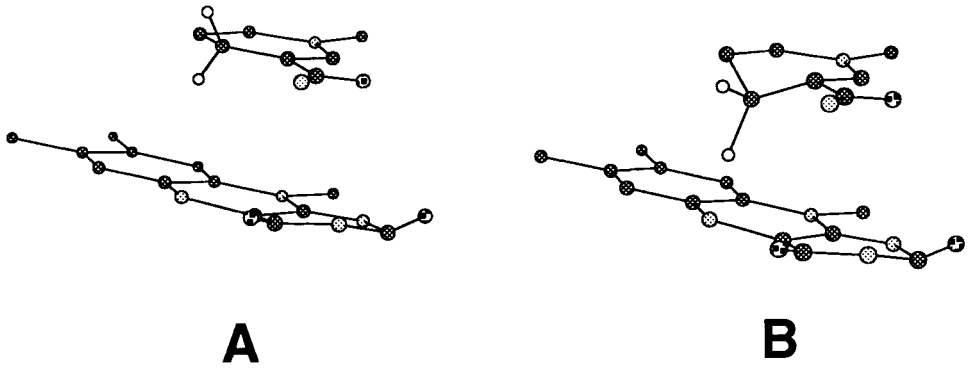

FIGURE 8: Possible orientation of NADPH in the active site of oxidized enzyme before reduction. (A) Schematic view of NADPH bound coplanarly in the active site above the flavin in the initial Michaelis complex, followed in (B) with the proposed puckering of the pyridine ring and lengthening of the C4−H bond to orient it more linearly with the π orbital of N5 in the isoalloxazine ring in the charge-transfer complex. Relative orientations are based loosely on the crystal structure of a similar complex in the EBP1 homologue, OYE1 (*41*). Structures were drawn using CS Chem3D, which represents carbon atoms in dark gray, nitrogen in light gray, oxygen in white with black squares, and hydrogen in solid white.

the subsequent effect on the stretching frequency of the C−H bond might explain the effects they noted (*35*).

With attention now turned to EBP1, the absence of an isotope effect on the association rate of the pyridine nucleotide substrate implies a minimal change of the conformation of the molecule in the Michaelis complex with the enzyme. The apparently substantial effect on the formation of the CT complex, on the other hand, may result from a combination of factors occurring in the transition state preceding it. The physical basis of the charge-transfer phenomenon is thought to require a very particular orientation of NADPH with respect to the flavin so that the energies of the relevant molecular orbitals are adjusted appropriately. Adopting such an orientation may introduce significant strain. For example, perhaps there is a pucker of the nicotinamide ring in order to align the axis of the C4-(pro-*R*-)H bond more linearly with N5 of the isoalloxazine ring of the flavin that presumably is oriented coplanarly in the initial complex (Figure 8). The fact that no significant effect was seen with the compound in which ^{2}H was substituted in the opposite diastereotopic position seems to indicate that the *pro-S* bond, in contrast, is not substantially affected in forming the CT complex.

As all microscopic constants reported here were derived primarily from simulation, the isotope effects observed on each microscopic step were not measured explicitly, and the interpretation of their magnitude requires some caution. Nevertheless, the values of the effects on the forward and reverse directions of CT formation appear to be 2.9 and 2.8, respectively, similar to a small primary effect, which seems consistent with the sum of distortion effects and a change in the stretching force constant of the C−H bond, as discussed above. The fact that normal effects are observed in both directions suggests that it is the transition state itself between the Michaelis and charge-transfer complexes where the largest changes (decreases) in the stretching force constant of the C4−H bond occur. The equilibrium effect of almost unity on CT formation suggests either little difference in the force constants of this bond between the "stable" intermediates themselves, or the involvement of other compensating factors that offset any real differences. For instance, it is possible that, as might be expected for an elongated C4−H bond, the symmetric stretch force constant is smaller in the CT than in the Michaelis complex, but is compensated for by a stiffening of other bending modes of this bond, so that the sum of effects results in an equilibrium effect near unity. Regardless of the exact values of the effects observed, there does not seem to be any other way to explain these data without invoking isotope effects on both charge-transfer formation and hydride transfer.

Results of earlier work with OYE should also be mentioned, though they are somewhat difficult to interpret because they involve enzyme prepared from brewer's yeast, which includes at least two different isozymes from the different yeast species present. Nevertheless, an analogous, albeit smaller, isotope effect was noted on the apparent rate of charge-transfer formation for that mixture of isozymes (*26*). It would be interesting to look for this type of effect with the purified, recombinant OYE's that are now available, especially as they display a wide range of affinities and turnover rates with NADPH.

With respect to the first half-reaction, it appears that EBP1 behaves most like the OYE2 isozyme, the primary OYE expressed in *S. cerevisiae* (*39*). Of the three OYE isozymes studied in detail, this is the only one that, like EBP1, binds NADPH too rapidly and tightly to measure in the stopped flow. Perhaps not surprisingly, this is the isozyme with which it shares the highest sequence homology, though at the amino acid sequence level it is not significantly higher than it is with the other isozymes (1% or less difference in identity between EBP1 and each isozyme, depending on alignment criteria) (*40*). There is not an obvious point in comparing the sequences with each other at which EBP1 and OYE2 can be set aside from the others, and so the rather drastic similarities and differences among the proteins in binding this substrate are probably the result of broader, subtler structural aspects. This is also supported by the crystal structure of OYE1 with an NADPH analogue, which reveals many and varied interactions between the enzyme and ligand, most of which occur outside the active site (*41*). In the paper that follows (*42*), the underlying structural elements of the reaction catalyzed by EBP1 are explored further, and it will be shown that there are significant mechanistic differences between EBP1 and the OYE's.

The identification of the physiological electron acceptor continues to be a major goal in our studies of EBP1. We have previously proposed that there may be an as yet undiscovered signaling pathway in *C. albicans* analogous

to the pathway in which OPDA reductase functions within *A. thaliana*, so that EBP1 serves a similar function, i.e., signal mediation, within this pathogenic fungus. This could lend congruence to the apparently associated phenomena of growth effects on the organism and the presence of environmental estrogens. Recently, another OPDA reductase was identified in tomato plant and shown to have the characteristic ligand binding properties of EBP1 and the OYE's (*12*), extending the functional similarity between the homologues, and illustrating the strict conservation of function across plant species. It remains a possibility that the conservation of this path and function extends to these yeast species.

ACKNOWLEDGMENT

We thank Drs. Stefan Engst, Judith Klinman, and Vincent Massey for helpful discussion.

REFERENCES

1. Powell, B. L., Frey, C. L., and Drutz, D. J. (1984) *Exp. Mycol. 8*, 304−313.
2. Gujjar, P. R., Finucane, M., and Larsen, B. (1997) *Ann. Clin. Lab. Sci. 27*, 151−156.
3. White, S., and Larsen, B. (1997) *Cell. Mol. Life Sci. 53*, 744−749.
4. Buckman, J., and Miller, S. M. (1998) *Biochemistry 37*, 14326−14336.
5. Buckman, J., Miller, S. M., Malloy, P., and Feldman, D. (1996) in *Twelfth International Symposium on Flavins and Flavoproteins* (Stevenson, K. J., Massey, V., and Williams, C. H., Jr., Eds.) pp 81−84, University of Calgary Press, Calgary.
6. Kinsman, O. S., and Collard, A. E. (1986) *Infect. Immun. 53*, 498−504.
7. Baron, S., and Hylemon, P. B. (1995) *Biochim. Biophys. Acta 1249*, 145−154.
8. French, C. E., and Bruce, N. C. (1995) *Biochem. J. 312*, 671−678.
9. French, C. E., Nicklin, S., and Bruce, N. C. (1996) *J. Bacteriol. 178*, 6623−6627.
10. Miura, K., Tomioka, Y., Suzuki, H., Yonezawa, M., Hishinuma, T., and Mizugaki, M. (1997) *Biol. Pharm. Bull. 20*, 110−112.
11. Schaller, F., and Weiler, E. W. (1997) *J. Biol. Chem. 272*, 28066−28072.
12. Strassner, J., Furholz, A., Macheroux, P., Amrhein, N., and Schaller, A. (1999) *J. Biol. Chem. 274*, 35067−35073.
13. Warburg, O., and Christian, W. (1932) *Naturwissenshaften 20*, 688−696.
14. Schopfer, L. M., and Massey, V. (1986) in *A Study of Enzymes* (Kuby, S. A., Ed.) pp 247−269, CRC Press, Boca Raton.
15. Stott, K., Saito, K., Thiele, D. J., and Massey, V. (1993) *J. Biol. Chem. 268*, 6097−6106.
16. French, C. E., and Bruce, N. C. (1994) *Biochem. J.*, 97−103.
17. Brown, B. J., Deng, Z., Karplus, P. A., and Massey, V. (1998) *J. Biol. Chem. 273*, 32753−32762.
18. Ryerson, C. C., Ballou, D. P., and Walsh, C. (1982) *Biochemistry 21*, 1144−1151.
19. Bergmeyer, H. U., Bernt, E., Schmidt, F., and Stork, H. (1974) in *Methods of Enzymatic Analysis* (Bergmeyer, H. U., Ed.) Vol. 3, pp 1196−1201, Academic Press, New York.
20. Harris, C. M., and Massey, V. (1997) *J. Biol. Chem. 272*, 22514−22525.
21. Strickland, S., Palmer, G., and Massey, V. (1975) *J. Biol. Chem. 250*, 4048−4052.
22. Barshop, B. A., Wrenn, R. F., and Frieden, C. (1983) *Anal. Biochem. 130*, 134−145.
23. Zimmerle, C. T., and Frieden, C. (1989) *Biochem. J. 258*, 381−387.
24. Franklund, C. V., Baron, S. F., and Hylemon, P. B. (1993) *J. Bacteriol. 175*, 3002−3012.
25. Porter, D. J., and Bright, H. J. (1980) *J. Biol. Chem. 255*, 7362−7370.
26. Massey, V., and Schopfer, L. M. (1986) *J. Biol. Chem. 261*, 1215−1222.
27. Miller, S. M., Moore, M. J., Massey, V., Williams, C. H., Jr., Distefano, M. D., Ballou, D. P., and Walsh, C. T. (1989) *Biochemistry 28*, 1194−1205.
28. Moore, J. W., and Pearson, R. G. (1981) *Kinetics and Mechanism*, Third ed., John Wiley & Sons, New York.
29. Gassner, G., Wang, L., Batie, C., and Ballou, D. P. (1994) *Biochemistry 33*, 12184−12193.
30. Schopfer, L. M., and Massey, V. (1980) *J. Biol. Chem. 255*, 5355−5363.
31. Fisher, H. F., and Saha, S. K. (1996) *Biochemistry 35*, 83−88.
32. Stewart, R. C., and Massey, V. (1985) *J. Biol. Chem. 260*, 13639−13647.
33. Chakroborty, S., Murthy, Y. V. S. N., and Massey, V. (1996) in *Twelfth International Symposium on Flavins and Flavoproteins* (Stevenson, K. J., Massey, V., and Williams, C. H., Jr., Eds.) pp 131−134, University of Calgary Press, Calgary.
34. Craig, D. H., Moody, P. C. E., Bruce, N. C., and Scrutton, N. S. (1998) *Biochemistry 37*, 7598−7607.
35. LaReau, R. D., Wan, W., and Anderson, V. E. (1989) *Biochemistry 28*, 3619−3624.
36. Bush, K., Mahler, H. R., and Shiner, V. J., Jr. (1971) *Science 172*, 478−480.
37. Cleland, W. W. (1980) *Methods Enzymol. 64*, 104−125.
38. Cook, P. F., Oppenheimer, N. J., and Cleland, W. W. (1981) *Biochemistry 20*, 1817−1825.
39. Niino, Y. S., Chakraborty, S., Brown, B. J., and Massey, V. (1995) *J. Biol. Chem. 270*, 1983−1991.
40. Madani, N., Malloy, P., Rodriguez-Pombo, P., Krishnan, A., and Feldman, D. (1994) *Proc. Natl. Acad. Sci. U.S.A. 91*, 922−926.
41. Fox, K. M., and Karplus, P. A. (1994) *Structure 2*, 1089−1105.
42. Buckman, J., and Miller, S. M. (2000) *Biochemistry 39*, 10532−10541.

BI0006520